Simulating Heat Stress of Coal Gangue Spontaneous Combustion on Vegetation Using Alfalfa Leaf Water Content Spectral Features as Indicators

Qiyuan Wang
China University of Mining and Technology - Beijing Campus
Yanling Zhao (ylzhao@cumtb.edu.cn)
China University of Mining and Technology - Beijing Campus https://orcid.org/0000-0002-6701-754X
Feifei Yang
China Agricultural University
Tao Liu
Yangzhou University Agricultural College
Wu Xiao
Zhejiang University
Haiyuan Sun
China University of Mining and Technology - Beijing Campus

Research

Keywords: heat stress, live fuel moisture content, spectral features, long-short-term memory

Posted Date: April 20th, 2021

DOI: https://doi.org/10.21203/rs.3.rs-426563/v1

Simulating heat stress of coal gangue spontaneous combustion on vegetation using alfalfa leaf water content spectral features as indicators

Qiyuan Wang[1], Yanling Zhao[1 *], Feifei Yang[2], Tao Liu[3], Wu Xiao[4], Haiyuan Sun[1]

[1] *Institute of Land Reclamation and Ecological Restoration, China University of Mining & Technology (Beijing), Beijing 100083, P.R. China*

[2] *College of Information and Electrical Engineering, China Agricultural University, Beijing 100083, P.R. China*

[3]*Jiangsu Key Laboratory of Crop Genetics and Physiology/Co-Innovation Center for Modern Production Technology of Grain Crops; Agricultural College, Yangzhou University, Yangzhou 225009, P.R. China*

[4]*Department of Land Management, Zhejiang University, Hangzhou 310058, P.R. China*

Note: The character "*" means that author is corresponding authors.

Abstract

Background: Vegetation heat-stress assessment in the reclamation areas of coal gangue dumps is of great significance in controlling spontaneous combustion. **Methods:** The study simulated the heat-stress environment of a coal gangue dump reclamation area through a temperature gradient experiment. We collected leaf spectrum and water content data on alfalfa plants commonly planted in such areas. We then obtained the optimal spectral features of appropriate leaf water content indicators through time series analysis, correlation analysis, and least absolute shrinkage operator (lasso) regression analysis. A spectral feature-based long short-term memory (SF-LSTM) model is proposed to estimate alfalfa's heat stress level. **Results:** Comparing three leaf water content indicators, we found that the live fuel moisture content (LFMC) varies significantly with time and has high regularity. Correlation analysis of the raw spectrum,

first-derivative spectrum, vegetation indexes and leaf water content data shows that LFMC and spectral data were the most strongly correlated. Combined with lasso regression analysis, the optimal spectral features were the first-derivative spectral value at 1661 nm (abbreviated as FDS (1661)), RVI (1525, 1771), DVI (1412, 740) and NDVI (1447,1803). When the classification strategies were divided into three categories and the time sequence length of the spectral features was set to five consecutive monitoring dates, the SF-LSTM model had the highest accuracy in estimating the heat stress level in alfalfa. The accuracy of the training set was > 95% and the accuracy of the verification set was about 90%. **Conclusion:** The results provide an important theoretical basis and technical support for vegetation heat-stress assessment in coal gangue dump reclamation areas.

Keywords: heat stress, live fuel moisture content, spectral features, long-short-term memory

Background

The organic materials in coal gangue dumps can oxidize and generate heat, such that spontaneous combustion may occur when the rate of heat generation exceeds that of heat dissipation [1-2]. The spontaneous combustion of coal gangue dumps poses a serious threat to the environment and human safety. This spontaneous combustion, by releasing a large number of toxic and harmful gases and chemical [3], damages the surrounding soil and water environment in the mining area [4-5]. It may also cause geological disasters during the long-term stacking [6], resulting in human casualties. In 2005, a coal gangue hill in China, spontaneously ignited, resulting in the death of eight people and burns to 122 people [7]. Further, over 30 miners were killed in the Ukraine from an explosion due to spontaneous combustion of coal in 2014 [8]. Remediation of coal gangue dumps mainly involves land reclamation and ecological reconstruction to reduce the probability of spontaneous combustion and other disasters [9]. A warning of spontaneous combustion in coal gangue dump reclamation areas helps managers take

45 effective and timely countermeasures. Remote sensing can be used for this purpose. Research this type
46 of monitoring has mostly focused on surface temperature and coal fire monitoring via thermal infrared
47 sensing [10-15]. However, changes in surface temperature are greatly affected by climate, sunshine, and
48 other factors, which cause high hysteresis in spontaneous coal fire monitoring and make it impossible to
49 obtain reliable early warnings. It has been found that prior to spontaneous combustion in coal gangue
50 dumps, there is an internal heat accumulation stage that can affect the growth of plants. In this stage,
51 there is potential to gain an early warning based on the spectral responses of plants. By averting
52 spontaneous combustion disasters, the ecological environments of mining areas can be fundamentally
53 improved.

54 Heat accumulation inside gangue dumps increases the surface soil temperature, which can reduce
55 root numbers, roots' absorption of water and nutrients, and plant fresh weights [16]. High soil
56 temperature is far more influential than high air-temperature on plant growth [17]. At present, few studies
57 have used remote sensing to monitor soil heat stress, and have mainly focused on drought stress [18],
58 waterlogging stress [19], high-temperature stress [20], disease stress and heavy metal stress [21]. Plant
59 environmental stress has been estimated directly or indirectly based on spectral features (such as
60 frequency-domain transformation features [22], vegetation indexes [23]), physiological and biochemical
61 parameters (such as plant water [24], the leaf area index [25], pigment content [26], and chlorophyll
62 fluorescence parameters [27])

63 The heat stress caused by internal spontaneous combustion may eventually evolve into a fire in coal
64 gangue dump reclamation areas. In such scenarios, the monitoring of plant water status is an important
65 factor in detecting temperature anomalies [28]. Remote sensing can monitor plant water content because
66 plant water absorbs radiation in the near-infrared (750–1300 nm) and short-wave-infrared (1300–2500

67 nm) regions [29]. Research has found that equivalent water thickness (EWT [18]), LFMC [30], and the
68 relative water content (RWC [31]) of leaves can better reflect vegetation water status. Currently,
69 commonly used vegetation moisture inversion methods include radiation transfer model inversion [32-
70 34], traditional regression models [35-37], and machine learning models [38]. Yebra M et al. [39] used
71 radiation transfer model inversion to estimate fuel moisture contents from MODIS reflectivity data and
72 established a flammability index through logistic regression modeling to map fire risk in Australia. Yi Q
73 et al. [40] reported that DR1647/DR1133 and DR1653/DR1687 (DR = first-order differential reflectance
74 value) are the optimal indexes for estimating EWT and LFMC, respectively. Rodríguez-Pérez JR et al.
75 [35] used near-ground hyperspectral data to estimate grape leaf water content and used ordinary least-
76 squares regression (OLSR) and functional linear regression (FLR) modeling, finding that the FLR model
77 centered at 1465 nm had the highest accuracy (R^2 = 0.7, RMSE = 8.485). Krishna G et al. [41] predicted
78 RWC according to the water deficit stress status of rice genotypes based on spectral indices, multivariate
79 techniques, neural network techniques, and existing water-band indices. They proposed new water-band
80 indices—the ratio index (RI) and normalized difference ratio index (NDRI)—for this purpose. In
81 previous studies, the water indicators obtained by remote sensing technology have been used to
82 qualitatively analyze plant water condition over an entire monitoring period to determine environmental
83 stress level on vegetation. However, the accuracy and timeliness of the results are usually insufficient.
84 In this paper, a long-short-term-memory network model based on spectral features is proposed to
85 estimate heat stress. It simulates the temperature-gradient test of plant heat stress in coal gangue dump
86 reclamation areas and monitors plant water condition based on hyperspectral remote sensing. This
87 provides a new way to monitor spontaneous combustion in coal gangue dumps. This method considers
88 temporal variation in the spectral features of water status in vegetation under environmental stress. It

allows accurate diagnoses to be made soon as possible and provides a new method of remote sensing monitoring of other environmental stresses.

Materials and methods

Experimental design

The simulation experiment was carried out in the autumn of 2020 at the potted proving ground of Yangzhou University, Yangzhou, China (119° 25′ N, 32° 23′ E). Yangzhou is in the transition zone between the humid subtropical monsoon climate and the temperate monsoon climate. It has four distinct seasons and abundant sunshine and rainfall. Alfalfa, a common herbaceous plant commonly used in the reclamation areas of coal gangue dumps, was selected as the experimental plant. The species used was Algonquin [42].

Seeds were sown on September 10, 2020, at a sowing density of 10 holes per pot and two seeds per hole. Ten seedlings per pot were grown to the three-leaf stage and harvested on November 15, 2020. The inner diameter of the bottom of the barrel was 20 cm, the inner diameter of the mouth was 28 cm, the height of the pots was 31.5 cm, and the empty barrel weighed 0.54 kg. Each barrel was loaded with 10 kg air-dried light loam and 5.28 g compound fertilizer with an N-P-K ratio of 15%-15%-15%. One kg of soil was used to cover the seeds after sowing. The first alfalfa crop took about 60 days to grow from the sowing to the flowering stage. The gradient experiment of heat stress was started on October 16, 2020. One control group and five experimental groups were set. For the experimental groups, five heat sources of different temperature T (T1 = 60 ℃, T2 = 90 ℃, T3 = 120 ℃, T4 = 150 ℃, and T5 = 180 ℃) were placed at a depth of 30 cm in the soil layer, which is the typical thickness of overlying soil used in reclamation projects [43] (Fig. 1(b)). Each group was replicated five times, as shown in Fig. 1(a). The relative water content of all treated soils was controlled at about 60%.

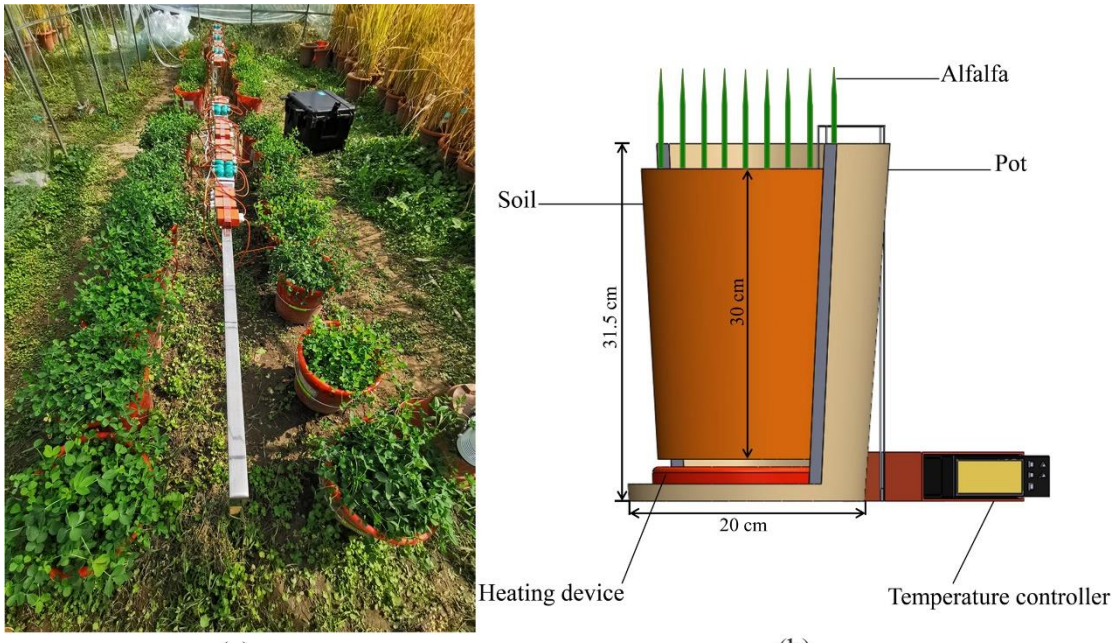

Fig.1 (a) Field of simulation experiment of heat stress in alfalfa and (b) schematic diagram of the heating equipment.

Data acquisition

Spectral data

A portable ground object spectrometer (Spectra Vista Corporation SVC HR-1024I) was used to measure the spectral reflectance of alfalfa leaves. The spectral measurement range was 340–2500 nm and the spectral sampling intervals were 1.5 nm (sampling range 350–1000 nm), 3.8 nm (sampling range 1000–1885 nm), and 2.5 nm (sampling range 1885–2500 nm). The resample interval was 1 nm. The measurements were synchronized with the heating. The first measurement was made on October 16, 2020, and then every 4 days. The spectral reflectance of leaves was measured between 10:00 and 14:00 on sunny and windless days. The spectral data were collected eight times until November 15, 2020, when it was overcast and rainy. A standard whiteboard was used for calibration of measurements using a hand-held leaf spectrum detector with a light source. This was clamped to the middle part of a leaf sample to measure its spectrum. Each process measured three pots and each pot was measured six times, with the

126 average taken as the processed alfalfa leaf spectrum reflectance. During the measurement process,
127 standard whiteboard calibration was performed every 30 minutes.

128 **Leaf water content**

129 Leaf water content data were collected synchronously with spectral data. Three alfalfa samples were
130 selected for each treatment and packed in self-sealing plastic bags to avoid water loss from the plants as
131 much as possible. Samples were quickly brought back to the laboratory to weigh their fresh weight (m_f)
132 with a precision balance and manually measure their leaf area. Each treated fresh leaf was put into a
133 beaker filled with distilled water and soaked for 24 hours. After reaching a constant weight, the saturated
134 fresh weight was measured (m_t). Then a blade put into the paper bag, which was placed in an oven at
135 105 ℃ for 30 min, then the drying temperature was set at 80 ℃ for 48 h until the constant weight was
136 attained, which was measured as the dry weight (m_d). The leaf water content was calculated according
137 to Eqs. (1), (2), and (3):

138

139 $$LFMC = \frac{m_f - m_d}{m_d} \quad (1)$$

140 Where m_f is the measured weight of fresh leaves and m_d is the weight of the same sample after
141 drying.

142 .

143 $$EWT = \frac{m_f - m_d}{A} \quad (2)$$

144 Where A is the leaf area.

145 $$RWC = \frac{m_f - m_d}{m_t - m_d} \quad (3)$$

146 Where m_t is the measured saturation weight of the leaves.

Methods

Spectral feature construction

Raw spectral data processing: Matlab 2017a (Mathworks, Natick, Massachusetts, USA) was used to average the spectral curves collected for each treatment in the heat-stress test to reduce the differences within groups. Then, a one-dimensional Gaussian filter was applied to the mean spectral curve along the spectrum direction to smooth it. The sliding window was set to 5, as shown in Figure 2.

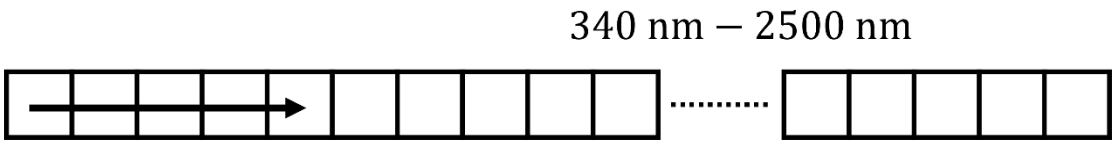

Fig. 2 Schematic diagram of one-dimensional Gaussian filtering along the spectrum direction, with a sliding window of 5.

First derivative spectrum: Differential processing of a spectrum can reduce the influence of background information such as field noise and soil on spectral data [44]. The direct difference method was used to calculate the first-derivative spectrum of spectral reflectance to highlight the target spectral features. Eq. (4) was used to calculate the first derivative of the spectrum.

$$\rho'(\lambda_i) = [\rho(\lambda_i + 1) - \rho(\lambda_i - 1)] / 2\Delta\lambda \quad (4)$$

In the formula, λ_i is the wavelength, $\rho(\lambda_i)$ and $\rho'(\lambda_i)$ are the reflectance and first-derivative spectrum of the wavelength λ_i, respectively, and $\Delta\lambda$ $\Delta\lambda$ is the interval between the wavelength $\lambda_i - 1$ and λ_i.

Vegetation index: The vegetation index was constructed using the two-band combination method of raw and first-derivative spectral reflectance, and compared with the conventional vegetation index (Table 1). The two-band combination method included the ratio vegetation index ($RVI(\lambda_1, \lambda_2)$), normalized difference vegetation index ($NDVI(\lambda_1, \lambda_2)$), and difference vegetation index

($DVI\ (\lambda_1,\ \lambda_2)$). These are commonly used in remote sensing monitoring. The selection range of any band combination was between 340–2500 nm and their formulas [45] are as follows:

$$NDVI\ (\lambda_1,\ \lambda_2) = (R_{\lambda_1} - R_{\lambda_2}) / (R_{\lambda_1} + R_{\lambda_2}) \quad (5)$$

$$RVI\ (\lambda_1,\ \lambda_2) = R_{\lambda_1} / R_{\lambda_2} \quad (6)$$

$$DVI\ (\lambda_1,\ \lambda_2) = R_{\lambda_1} - R_{\lambda_2} \quad (7)$$

Where λ_1 and λ_2 are wavelengths (nm); and R_{λ_1} and R_{λ_2} are the reflectances at wavelengths λ_1 and λ_2, respectively, and $\lambda_1 \neq \lambda_2$.

Table1 Vegetation indices related to leaf water content.

Vegetation index	Acronym	Equation[1]	Reference
Water index	WI (900, 970)	R_{900} / R_{970}	[46]
Water index	WI (1300, 1450)	R_{1300} / R_{1450}	[47]
Normalized difference water index	NDWI	$(R_{870} - R_{1260}) / (R_{870} + R_{1260})$	[48]
Normalized difference vegetation index	NDVI	$(R_{858} - R_{645})/(R_{858} + R_{645})$	[49]
Normalized difference infrared index	NDII	$(R_{858} - R_{645}) / (R_{858} + R_{645})$	[50]
Simple ratio vegetation index	SR	R_{800} / R_{680}	[51]
Moisture stress index	MSI	R_{1610} / R_{842}	[52]
Photochemical reflectance index	PRI	$(R_{570} - R_{531}) / (R_{570} + R_{531})$	[53]

[1] R_λ = reflectance at wavelength λ

Spectral feature selection

Correlation analysis: The Pearson correlation coefficient (Eq. (8)) was used to correlate the spectral parameters (raw spectrum, first-derivative spectrum, and vegetation index) with plant leaf water content indicators (LFMC, EWT, and RWC). Pairwise analysis selected highly correlated spectral features in the

appropriate band range.

$$r(X,Y)=\frac{Cov(X,Y)}{\delta_X \delta_Y} \tag{8}$$

Where $Cov(X,Y)$ is the covariance of X and Y, δ_X is the variance of X, and δ_Y is the variance of Y.

Lasso regression: The Lasso regression model was proposed by Robert in 1996 and has become an important regression model in the field of machine learning [54]. The method is a compression estimator that constructs a penalty function to obtain a relatively refined model. This makes it compress some regression coefficients; that is, the sum of the absolute value of the forcing coefficient is less than a fixed value. Through regularization, the regression coefficients of some independent variables are compressed to zero, then the variable selection is completed. At the same time, Lasso regression retains the advantage of subset contraction and is a biased estimation model (Eq. (9)) for dealing with data with multicollinearity.

$$\min_{\beta_0,\beta}\left(\frac{1}{2N}\sum_{i=1}^{N}(y_j-\beta x_i^T-\beta_0)+\lambda\sum_{j=1}^{p}|\beta_j|\right) \tag{9}$$

Where N is the sample number, y_j is the predicted true value, x_i is the observed value, β_0 is the bias, β is the weight of the observed variable, and λ is a non-negative regularization parameter. $\lambda\sum_{j=1}^{p}|\beta_j|$ is called L^1 regularization.

Assessment of heat stress by SF-LSTM

LSTM is a recurrent neural network (RNN) architecture used in the field of deep learning, and was proposed by [55]. Unlike standard feedforward neural networks, LSTM has a feedback connection. It not only processes point datasets (such as images) but also processes data sequences. Compared with other deep learning algorithms, LSTM performs very well in processing regression or classification problems with time series feature data and is now widely used. The characteristics of temporal change in

physiological parameters must be taken into account when estimating environmental stress level, and the influence of subjective qualitative analysis on the estimation accuracy should be avoided as far as possible. Therefore, in this paper, based on the multi-dimensional and multi-time-series characteristics of the test plant moisture indicators, Pytorch (Facebook AI Research, Menlo Park, California, USA) was used to construct the artificial RNN SF-LSTM. Its structure is shown in Figure 3.

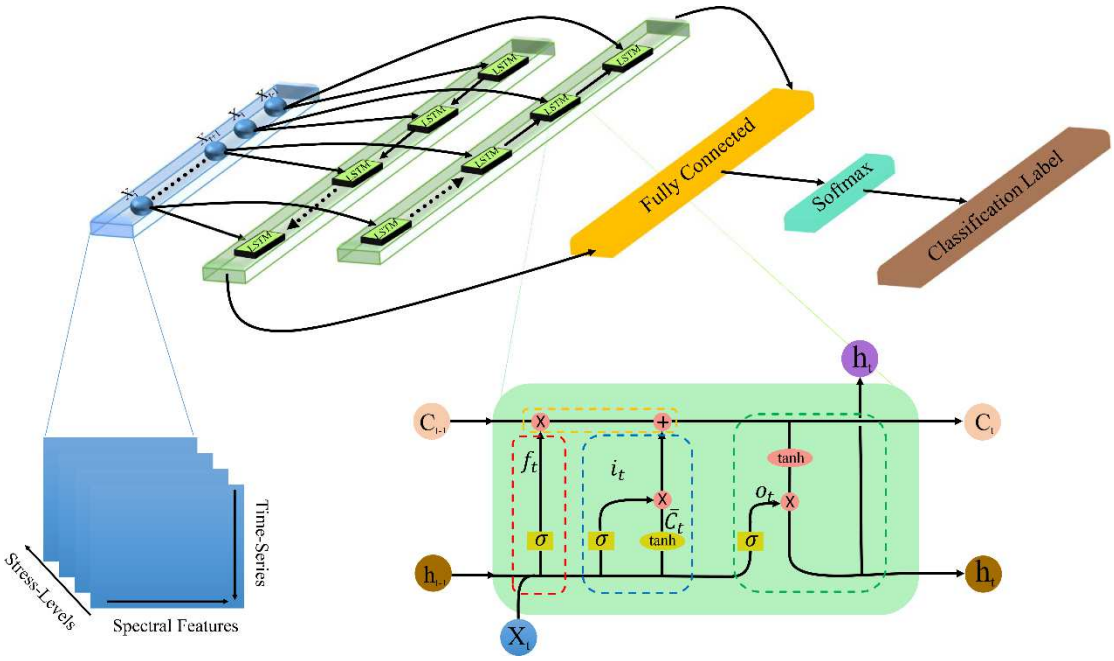

Fig. 3 SF-LSTM network structure diagram.

SF-LSTM is a neural network model based on bidirectional LSTM and uses spectral features as the input layer. The whole network is composed of an input layer, bidirectional LSTM layer, full connection layer, Softmax layer, and classified output layer. At the lower left of Fig. 3, the data structure of the input layer is enlarged. Inspired by image data processing, a three-dimensional matrix was constructed with dimensions of 1) spectral features, 2) time-series, and 3) stress level. The data structure of the input layer not only considers the calculation of various spectral features but also ensures that the data can be calculated according to the time series. At the same time, the multi-dimensional vector operation makes the calculation efficient. The core computing units, called *memory*

cells, are zoomed in at the lower right of Fig. 3. In the memory cells, "⊗" and "⊕" denote the dot product and matrix addition, respectively. The first step of the memory cell is to decide what information to discard from the cellular state. This decision is made by a sigmoid layer called the "forget gate". It looks at h_{t-1} (the previous output) and X_t (the current input), and outputs a number between 0 and 1 for each number in C_{t-1} (the previous state), where 1 represents total retention and 0 represents total deletion (Eq. (10)). The next step is to decide what information to store in the cellular state. The sigmoid layer called the "input gate" decides which values to update, and the next tanh layer creates a candidate vector $\tilde{C}_t$ (Eqs. (11), (12)), which is added to the state of the cell and combined with C_{t-1} to create the updated value C_t (Eq. (13)). Finally, the "output gate" determines the output of the memory cells. The output value of h_t is obtained by multiplying the output of a sigmoid layer with the normalized C_t value of the tanh layer (Eqs. (14), (15)).

$$f_t = \sigma(W_f \cdot [h_{t-1}, X_t] + b_f) \tag{10}$$

$$i_t = \sigma(W_i \cdot [h_{t-1}, X_t] + b_i) \tag{11}$$

$$\tilde{C}_t = \tanh(W_c \cdot [h_{t-1}, X_t] + b_c) \tag{12}$$

$$C_t = f_t * C_{t-1} + i_t * \tilde{C}_t \tag{13}$$

$$o_t = \sigma(W_o \cdot [h_{t-1}, X_t] + b_o) \tag{14}$$

$$h_t = o_t * \tanh(C_t) \tag{15}$$

where σ is the logistic sigmoid function, W is the weight matrix, $*$ is a dot product, and b is a bias term.

Validation

The observed sample data for constructing the model was divided into a training set (segmentation scale = 0.8) and validation set (segmentation scale = 0.2). The coefficient of determination (R^2) and root mean

240 square error (RMSE) were used as indicators of its accuracy [24] Eqs. (16), (17)). Accuracy is defined
241 as the degree of consistency between the model results and the true categories (Eq. (18)). Ten-fold cross-
242 validation was adopted for the training set [56].

243 $$RMSE = \sqrt{\frac{\sum_{i=1}^{n}(\hat{y}_i - y_i)^2}{n}} \quad (16)$$

244 $$R^2 = 1 - \frac{\sum_{i=1}^{n}(\hat{y}_i - y_i)^2}{\sum_{i=1}^{n}(\overline{y}_i - y_i)^2} \quad (17)$$

245 $$Accuracy = \frac{n_{class}}{n} \times 100\% \quad (18)$$

246 Where y_i is the true value, $\hat{y}_i$ is the predicted value, $\overline{y}_i$ is the mean value, n is the number of
247 samples, and n_{class} is the number of correctly classified samples.

248 **Results**

249 **LFMC, EWT, and RWC time series analysis**

250 This study focused on alfalfa, a herbaceous plant commonly used in the reclamation areas of coal
251 gangue dumps. The soil layer was heated on the day after the first data collection on October 14, and
252 leaf samples were collected eight times in total. The changes in LFMC, EWT, and RWC with time
253 under different treatments are shown in Figure 4. The temporal changes in water indicators under
254 different heat stresses were different. The soil layer was not heated when the soil was collected on
255 October 14. At this time, the growth trend in each alfalfa pot was similar, and the differences in LFMC,
256 EWT, and RWC between each experimental group were small.

257 Figure 4 shows the following. 1) EWT: All treatments showed an overall growth trend. The
258 control group increased almost all the time, reaching the maximum value on November 11 before
259 dropping slightly on November 15. Apart from this overall trend, the EWTs of the other experimental
260 groups showed different trends with no strong regularity over time. 2) RWC: The differences between

261 groups on a particular date were small and the range of variation in RWC on different dates was
262 relatively stable. On November 7 and 11, the RWC of the control group and each experimental group
263 peaked. On November 15, the RWC of each treatment group declined, with a relatively large range of
264 decreases. In general, there was no significant difference in RWC between the control and experimental
265 groups. 3) LFMC: After heating the soil layer, the LFMCs of the control group were significantly
266 higher than those of the experimental groups on each monitoring date. The LFMCs of each
267 experimental group showed gradually decreasing trends. In the late monitoring period, the LFMC
268 decreased with increases in the temperature gradient on November 7, 11, and 15 and reached the lowest
269 point on November 15, exhibiting a clear decrease over time.

270 According to the results of water indicator monitoring and the above analysis, it is clear that
271 LFMC is the best water indicator for reflecting heat stress in alfalfa. This is consistent with previous
272 studies. LFMC is very sensitive to heat stress and is an important variable in many fire behavior
273 prediction models and fire-risk indicators [39,57].

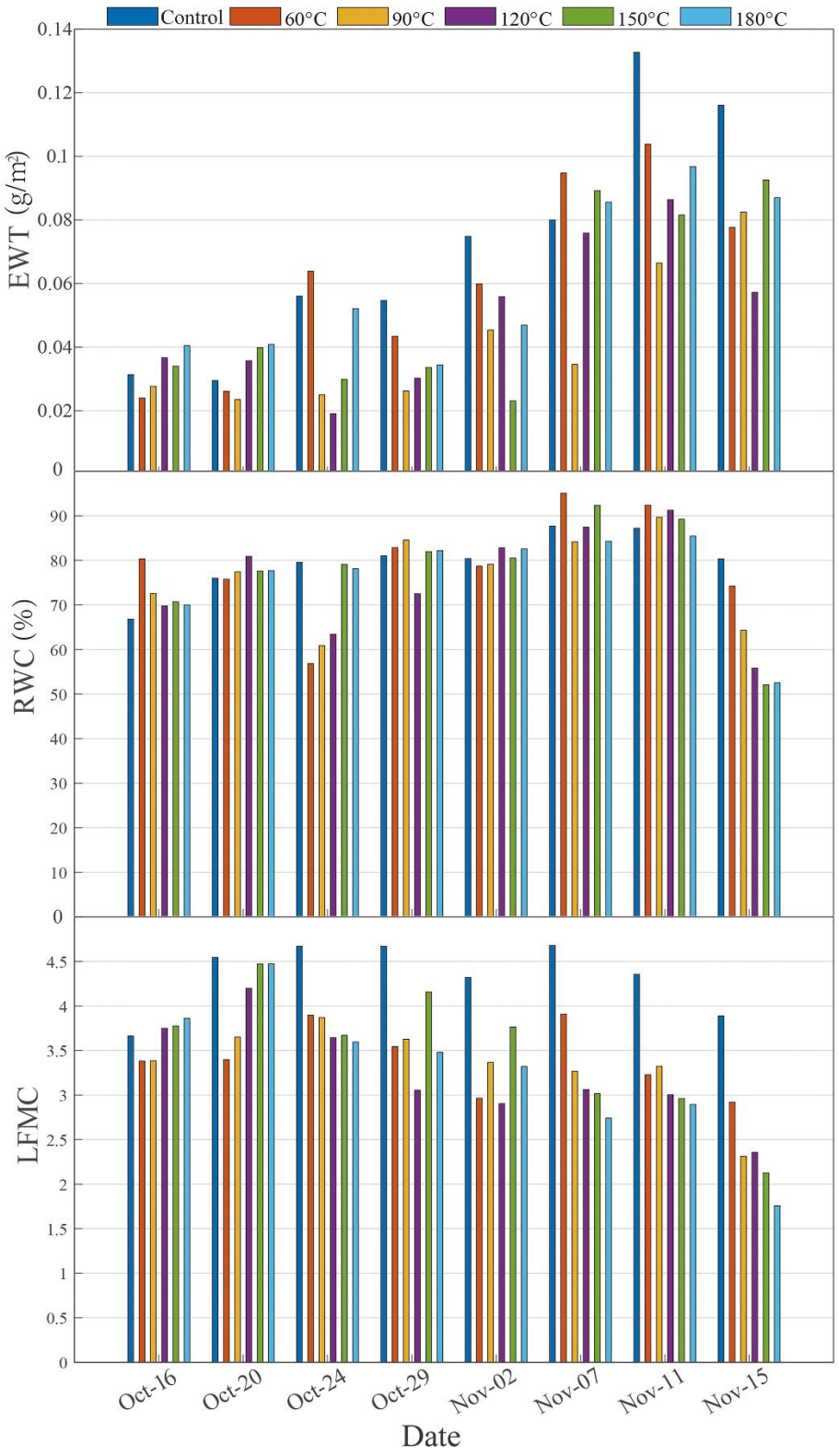

Fig.4 Time series of equivalent water thickness (EWT), live fuel moisture content (LFMC), and relative water content (RWC) in the control and experimental groups at leaf level from October 16–November 15, 2020.

Correlation analysis of spectral features and leaf water content

Correlations between raw spectrum, derivative spectrum, and leaf water content data

The Pearson correlation coefficient is one of the most commonly used indicators in correlation analysis [58], and was used in this paper. Correlation analysis of EWT, RWC, and LFMC was performed using raw leaf spectrum and first-derivative spectrum data from throughout the monitoring period (14 October–15 November; Fig. 5). The results show that the raw spectra of leaves were positively correlated with EWT at all wavelengths, negatively correlated with RWC except at a small number of visible wavelengths (VIS, 400–780 nm), and negatively correlated with LFMC at all wavelengths. Overall, the EWT, RWC, and raw spectrum correlations were weak ($|r| < 0.6$), of which the RWC was weaker, while LFMC was best in the short-wave infrared band (SWIR, 1400–2500 nm) to obtain the strong correlation band ($|r| > 0.7$), and the correlation was strongest at 1889 nm ($r = -0.75$). The first-derivative spectrum can effectively suppress influences such as the soil background. In the correlation analysis of the first-derivative spectrum, EWT and RWC, the positive and negative correlations were uncertain and the absolute values of the correlation coefficients were small. The performance of LFMC continued to be excellent, with the maximum correlation coefficient between LFMC and the first-derivative spectrum appearing at 1661 nm ($r = -0.77$).

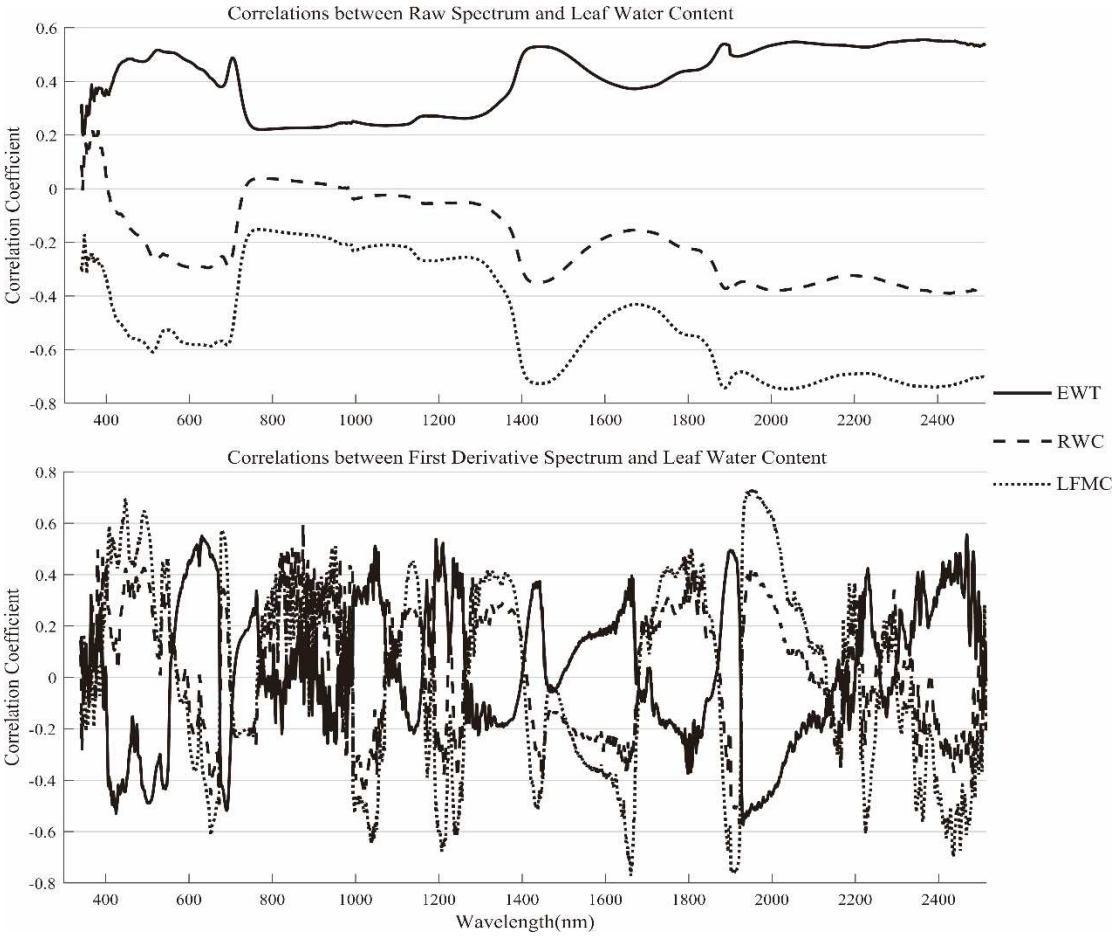

Fig.5 Coefficients of correlation between EWT, RWC, LFMC and the raw leaf and first-derivative spectral data

Correlation between vegetation index and leaf water content

In remote sensing monitoring of plant water content, vegetation indexes have been widely used and are some of the most important spectral parameters. Therefore, we first analyzed the correlations between eight classical vegetation indices and EWT, RWC, and LFMC (Table 2). The correlations between each index and EWT and RWC were weak. In contrast, the correlations between LFMC and each index were better. The vegetation indices with good correlations with LFMC comprised bands mainly concentrated in the near-infrared and SWIR regions. The WI (1300,1450), NDVI, and NDII had correlations with LFMC of > 0.6, among which the correlation between WI (1300,1450) and LFMC was the highest at 0.7. The results in Table 2 show that these classical vegetation indices are not quite adequate for

306 application in this paper, and a vegetation index with better correlation needs to be constructed.

307 **Table 2** Coefficients of correlation (*r*) between existing vegetation indices and leaf water content

Vegetation index	*r*			Vegetation index	*r*		
	EWT	RWC	LFMC		EWT	RWC	LFMC
WI (900,970)	0.34	-0.39	-0.64	NDWI	0.22	-0.57	-0.59
WI (1300,1450)	0.44	-0.39	-0.7	NDVI	0.39	-0.33	-0.57
SR	-0.37	-0.33	-0.57	NDII	0.33	-0.44	-0.63
MSI	-0.35	0.42	0.64	PRI	-0.44	0.31	-0.5

308 To find the best vegetation indices for estimating leaf water content, the correlations between the
309 ratio (RVI), normalized-difference (NDVI), and difference (DVI) vegetation indices of the two bands in
310 the 340–2500 nm range with EWT, RWC, and LFMC were systematically analyzed. Figure 6 presents a
311 matrix of the correlation coefficients based on the different band combinations of the raw full-band
312 spectrum and the leaf water content. The results show that the correlations between the vegetation indices
313 and EWT and RWC were still weak, with LFMC performing best, which is consistent with the previous
314 analysis. From Figs. 6 (g), (h), and (i), the three indices with the highest correlation coefficients *r* (RVI
315 (1525,1771), DVI (1412,740), and NDVI (1447,1803)) were screened out, with the *r*-values being 0.81,
316 0.82, and 0.77, respectively. The band compositions of the three vegetation indices are in the near-
317 infrared and SWIR, and they were highly correlated with the LFMC. Therefore, they can be preliminarily
318 used as the spectral characteristic parameters of the LFMC.

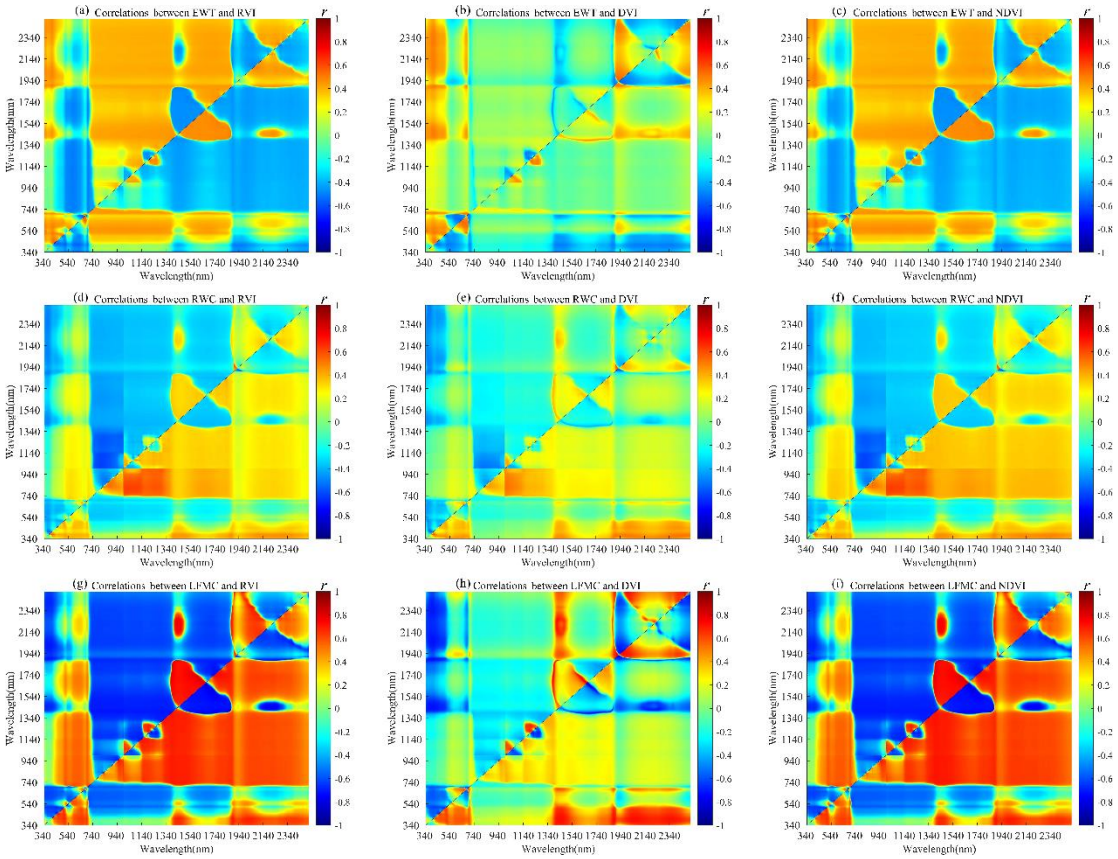

Fig. 6 Coefficients of correlation between EWT, RWC, and LFMC with RVI (λ1, λ2), NDVI (λ1, λ2), DVI (λ1, λ2), and ratio/normalized difference/difference vegetation indexes constructed from raw spectral data

Optimal spectral features

According to the temporal changes in leaf water content and the correlation analysis with the raw spectral data, first-derivative spectrum, and vegetation index, it is obvious that LFMC is the best water indicator for assessing heat stress, while EWT and RWC are not suitable. Based on correlation analysis, RS (1889; raw spectral value at 1889 nm), FDS (1661; first-derivative spectral value at 1661 nm), RVI (1525,1771), DVI (1412,740), and NDVI (1447,1803) were the five spectral features with strong correlations with LFMC. In general, selecting more features is not necessarily better, and data redundancy will reduce computational efficiency and affect the accuracy and applicability of the model. Therefore, it is necessary to further screen the spectral characteristic parameters of LFMC.

The regular term constructed in the Lasso regression model makes it possible to compress the dimension of the input sample. First, we need to determine the optimal regular coefficient Lambda (λ) and adopt 10-fold cross-validation for the dataset (Figure 7(a)). As shown in Fig. 7(a), the minimum λ of the RMSE was obtained after multiple iterations and was used as the regular term coefficient of the model. Then, the compressed spectral characteristic parameters were determined and the accuracy of the regression model was tested. The results are shown in Table 3 and Figure 7(b). It can be seen from Table 3 that RS (1889), as an independent variable, is compressed to 0 in the model, indicating that RS (1889) is removed from the input dimension. The R^2-value of the Lasso regression model constructed with FDS (1661), RVI (1525,1771), DVI (1412,740) and NDVI (1447,1803) as independent variables was 0.77 with an RMSE of 0.05. Although the spectral features were reduced, the model accuracy was still high.

Table 3 Correlation coefficients between existing vegetation indices and leaf water content

Lasso regression / Spectral parameters	Regression coefficients	R^2	RMSE
RS (1889)	0		
FDS (1661)	29		
RVI (1525,1771)	30.93	0.77	0.05
DVI (1412,740)	0.19		
NDVI (1447,1803)	-2.76		
Equation[1]	$y = 29x_1 + 30.93x_2 + 0.19x_3 - 2.76x_4$		

[1]y = LFMC; x_1 = FDS (1661); x_2 = RVI (1525,1771); x_3 = DVI (1412,740); x_4 = NDVI (1447,1803).

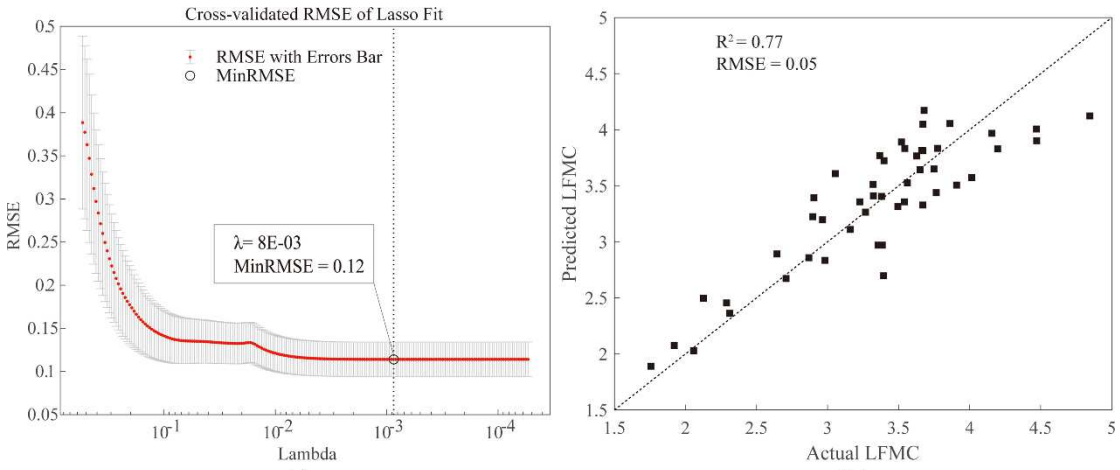

346

347 **Fig. 7** (a) Use of 10-fold cross-validation to determine the regular coefficient (lambda, λ) of the Lasso

348 model; (b) predicted and actual values of LFMC by Lasso regression.

349 **SF-LSTM estimation of heat-stress level**

350 The direct use of spectral characteristics to accurately estimate the stress level in plants requires full

351 consideration of the temporal changes in spectral data under different stress levels. Although it is

352 sometimes feasible to estimate the spectral data in a single period, its generalization ability is often

353 weak. To solve this problem, the spectral features of the time series were used as input to construct an

354 SF-LSTM, and the estimation of plant stress level was transformed into a classification problem. The

355 network structure is shown in Figure 4. To find the optimal model, the input layer data were set up with

356 unified spectral features and different time series lengths, and different classification strategies were

357 trialed: 1) Spectral features: FDS(1661), RVI(1525,1771), DVI(1412,740) and NDVI(1447,1803); 2)

358 time series: the time series length of spectral features was divided into lengths of 3, 5 and 7 (each

359 length is a continuous date and does not reverse repeat); 3) classification strategies: two categories

360 (control group and experimental groups), three categories (control group, T1 and T2, and T3, T4, and

361 T5) and six categories (control group and each of the five experimental groups). The number of

362 samples in each test was determined by the length of the time series, and the ratio of the training set to

363 the verification set was 4:1. The number of output layer categories was consistent with the number of
364 stress level categories. The initial learning rate was 0.01 and the batch size was adjusted according to
365 the sample size. The adaptive moment estimate (Adam) was selected by the network optimizer and the
366 cross-entropy error function was adopted as the loss function. The classification results are shown in
367 Figure 8.

368 When using deep learning to estimate the heat-stress level in terms of a binary classification or
369 multiple classification problem, the classification of categories has a huge impact on the modeling
370 results. The test results show that the classification strategy determines the convergence of the model's
371 loss and accuracy and the overall stability of the model. Under the same classification strategy, the time
372 series length of spectral features determines the level of model accuracy. As shown in Figure 8, among
373 the different classification strategies, the loss and accuracy of the dichotomy model converged, the
374 accuracies of the training set and evaluation set were not ideal, and the stability of the model was low.
375 When divided into six categories, the model cannot converge many times and its stability is very poor.
376 The heat-stress level was divided into three categories. The model training set had the highest accuracy
377 and the accuracy convergence value was > 95%. Under different time series lengths, the effect was not
378 good at a time series length of three. When the time series length of the data was five, the training set
379 loss and accuracy had good convergence. The evaluation set had high accuracy and good stability, and
380 its accuracy was stable at about 90%. Overfitting occurred at a time series length of seven. The overall
381 results show that the SF-LSTM model is suitable for estimating heat stress when the classification
382 strategies are divided into three categories and the time series length is five.

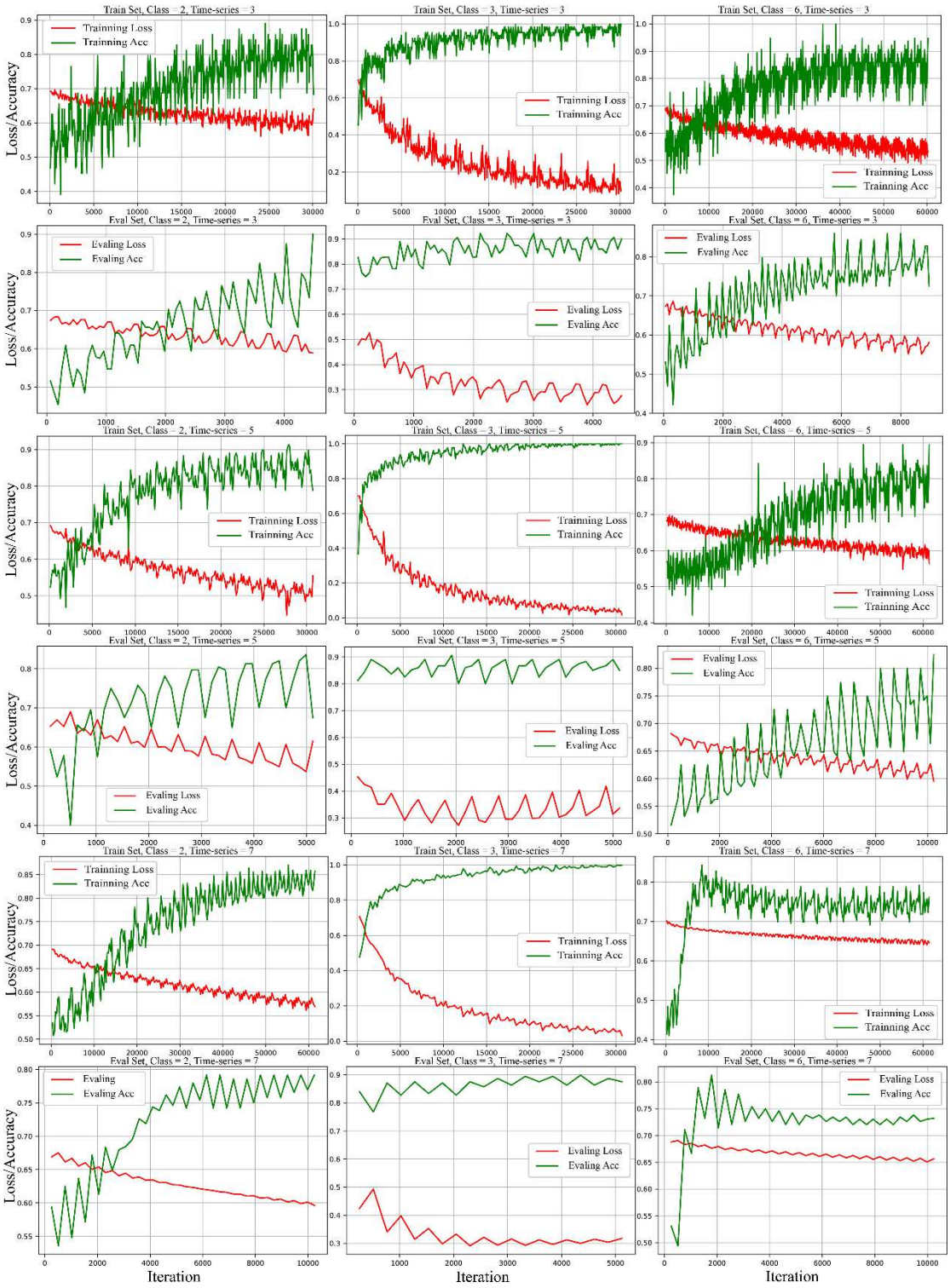

Fig. 8 Loss and accuracy of the SF-LSTM model training set and validation set under different classification strategies and time series lengths

Discussion

In this study, alfalfa was used to simulate thermal stress in a coal gangue dump reclamation area to

388 conduct a gradient test with several experimental groups (control group, T1 = 60 ℃, T2 = 90 ℃, T3 =
389 120 ℃, T4 = 150 ℃, T5 = 180 ℃). Water content and hyperspectral data on alfalfa leaves were collected
390 one month before the flowering period. Correlation analysis and selection of the spectral features of
391 alfalfa leaf water content were carried out. Based on the SF-LSTM model, the stress level in alfalfa under
392 heat stress was estimated.

393 **Leaf water content**

394 The LFMC showed obvious regularity under different temperature gradients, which may be due to the
395 calculations of LFMC and leaf dry and fresh weights. Root system growth has a huge impact on the dry
396 and fresh weights of the plant leaves. As the heat stress time increases, the supply of water and
397 nutrients to plant leaves becomes insufficient. Long-term high soil-temperatures cause significant
398 changes in the LFMC of plant leaves. Compared with high air-temperature, the photochemical
399 efficiency of leaves and the root growth of plants are more severely affected by stress due to high soil-
400 temperature. Kuroyanagi & Paulsen [17] also reported that shoot growth and senescence in winter
401 wheat are influenced more by soil-temperature than air-temperature. The adverse effects of high soil-
402 temperature on physiological activities are probably due to direct inhibition of root growth and activity
403 and, therefore, limitation of water and nutrient supplies to the leaves [59] and disruption of cytokinin
404 synthesis in roots [17, 60]. High soil-temperatures also promote leaf senescence by increasing the
405 transport of root abscisic acid (ABA) to the leaves [61]. Although there were fluctuations in EWT and
406 RWC during the monitoring period, the regularity was weak. This may be due to water shortages in the
407 plant leaves, lack of nutrients, and destruction of the internal microstructure of the leaves under
408 different degrees of high soil-temperatures [16], resulting in varying degrees of change in leaf area and
409 saturated water content.

Spectral features

Changes in leaf spectra are usually affected by changes in chlorophyll, water content, internal structure, dry matter content, etc. The reflectance spectra of green plants in the 1000–2500 nm region are mainly influenced by liquid water and dry compounds. The water absorption band is 1360–2080 nm, which is highly correlated with leaf water content and is not affected by leaf structure [62]. This study shows that the band sensitive to the leaf water content of alfalfa under high-soil-temperature heat stress is mainly concentrated in the long-wave infrared region (1400–2500 nm). Correlation analysis of the raw and first-derivative spectra with water content data showed that the bands at 1889 nm and 1661 nm had the highest correlations with LFMC, which was the optimal spectral feature (see Figure 3). This is similar to previous studies [63].

Due to the strong reflection from the surfaces of fresh leaves and the influences of the surface and internal structures of leaf cuticles, leaf hairs, etc., it is difficult to comprehensively and accurately estimate plant moisture status using a single band of spectral reflectance. By constructing a vegetation index, the effective spectral information of the vegetation can be maximized, the single-band scattering effect can be effectively reduced, and prediction accuracy can be improved [64]. This article analyzed the correlations between the ratio, difference, and normalized vegetation indexes and leaf water content in any two bands within 340–2500 nm. It found that the correlations between various indexes and LFMC were all high. Specifically, the three spectral features RVI (1525,1771), DVI (1412,740), and NDVI (1447,1803) had the highest correlations. The results of this part of the correlation analysis also verify that LFMC is the most suitable water content indicator for this study on temporal changes in leaf water content.

Through correlation analysis, we screened out several spectral features with strong correlations with

LFMC. However, in multiple regression, when the independent variable has a higher dimension, there are often problems such as collinearity and data redundancy [65]. Using the Lasso regression model to further optimize the above-mentioned spectral features can minimize the adverse effects of multi-dimensional input data on the assessment results when estimating the heat-stress level. After dimensionality reduction and Lasso regression, the spectral features selected in this paper were FDS (1661), RVI (1525,1771), DVI (1412,740), and NDVI (1447,1803).

Heat stress estimation

Considering the importance of temporal sequences in the estimation of plant environmental stress, LSTM (which can effectively utilize a temporal sequence of data in deep learning) was used to build an heat-stress model. Meanwhile, stress-level estimates were presented in the form of classification results for the application scenarios considered in this paper. Compared with traditional machine learning classification methods, LSTM is more effective in classifying remote sensing time series data [66]. A variety of classification strategies and time-series-length models were tested. The dichotomy strategy was the most common strategy used in the classification model. According to the results in Figure 8, although the parameters of the model constructed using the dichotomy strategy can converge, the accuracy was not acceptable. This may be related to the large difference in the proportion of the number of samples of the two categories in the training set and the evaluation set. In the next step of the study, this adverse factor was reduced by increasing the sample size of the control group during experimental data collection. Among the multi-classification strategies, three categories had the best effects. The longer the time series, the better. The model had the highest accuracy with a sequence length of five. This conclusion is in line with the laws of deep learning. Over-redundant data, complex neural network architectures, and inappropriate classification strategies not only make models unable to

fit the data, but also lead to over-fitting [67]. Over-fitted models have poor generalization ability and weak applicability.

Conclusions

In this study, an SF-LSTM model was established by using the time series spectral features of leaf water content obtained through an experiment that simulated heat stress in coal gangue dump reclamation areas. The model was effective in estimating the heat-stress level in alfalfa. Through time series analysis of leaf water content data, it was found that the EWT and RWC do not have high regularity over time, making it difficult to distinguish between normal and heat damage statuses in alfalfa. Heat stress in alfalfa was best indicated by the LFMC leaf water content index.

According to correlation analysis of the raw spectrum, first-derivative spectrum, three forms of vegetation index, and leaf water content data, RS(1889), FDS(1661), RVI(1525,1771), DVI(1412,740), and NDVI(1447,1803) had the strongest correlations with LFMC. After further screening by the Lasso regression model, FDS(1661), RVI(1525,1771), DVI(1412,740) and NDVI(1447,1803) were found to be the optimal spectral features of inversion LFMC, and can be used as spectral features to assess heat stress.

The SF-LSTM model was constructed to estimate the heat-stress level in alfalfa based on a time series of spectral features. The results show that this model can estimate the stress level with high accuracy when the classification strategies are divided into three categories (control group, T1 and T2, and T3, T4, and T5) and a spectral feature time series length of five (where the dates in the monitoring period are continuous without repetition).

The results of this study provide a new way to assess plant heat stress in coal gangue dump reclamation areas. This has important practical application value and is expected to be further verified

and applied in other types of environmental stress research. Subsequent studies will verify the conclusions of this experiment at larger spatial scales.

Abbreviations

Lasso: least absolute shrinkage operator; SF-LSTM: Spectral feature-based long short-term memory; LFMC: Live fuel moisture content; FDS: First-derivative spectral value; EWT: Equivalent water thickness; RWC: Relative water content; DR: First-order differential reflectance value; RI: Ratio index; NDRI: Normalized difference ratio index; RVI: Ratio vegetation index; NDVI: Normalized difference vegetation index; DVI: Difference vegetation index; WI: Water index; NDWI: Normalized difference water index; NDII: Normalized difference Infrared index; SR: Simple ratio vegetation index; MSI: Moisture stress index; PRI: Photochemical reflectance index; RNN: Recurrent neural network; VIS: Visible wavelengths; SWIR: Short-wave infrared band; RS: Raw spectral value; ABA: Abscisic acid.

Acknowledgments

This work was supported by the National Key Research and Development Program of China [grant numbers 2016YF C0501103-4, 2016YF C0501103-5]. The authors wish to express heartfelt thanks to Yang Tianle, Yao Zhaosheng, Zhang Weijun, and Lin Zihan for data acquisition work, and to Wang Dunliang and Li Rui for debugging the test equipment.

Authors' contributions

QW and FY: Conceptualization, methodology, data curation: Application of statistical, mathematical, computational, or other formal techniques to analyze or synthesize study data, Visualization, Writing-Original draft preparation. YZ and WX: Writing—review & editing, funding acquisition, conceptualization. TL and HS: Provision of study materials, laboratory samples, instrumentation. All authors read and approved the final manuscript.

Funding

This study was funded by the National Key Research and Development Program of China (2016YF C0501103-4, 2016YF C0501103-5).

Availability of data and materials

The processed data required to reproduce these findings cannot be shared at this time as the data also forms part of an ongoing study.

Declarations

Ethics approval and consent to participate

Not applicable.

Consent for publication

This manuscript has not been published elsewhere and is not under consideration by another journal.
Competing interests

This manuscript has no conflicts of interest to declare.

Author details

[1] Institute of Land Reclamation and Ecological Restoration, China University of Mining & Technology (Beijing), Beijing 100083, P.R. China. [2] College of Information and Electrical Engineering, China Agricultural University, Beijing 100083, P.R. China. [3] Jiangsu Key Laboratory of Crop Genetics and Physiology/Co-Innovation Center for Modern Production Technology of Grain Crops; Agricultural College, Yangzhou University, Yangzhou 225009, P.R. China. [4] Department of Land Management, Zhejiang University, Hangzhou 310058, P.R. China

References:

1.Sýkorová I, Pickel W, Christanis K, et al. Classification of huminite—ICCP System 1994. Int J Coal Geol. 2005;62:85-106.

2.Bian Z, Dong J, Lei S, et al. The impact of disposal and treatment of coal mining wastes on environment and farmland. Environmental geology. 2009;58:625-634.

3.Wu Y, Yu X, Hu S, et al. Experimental study of the effects of stacking modes on the spontaneous combustion of coal gangue. Process Saf Environ. 2019;123:39-47.

4.Zhengfu B, Inyang HI, Daniels JL, Frank O, Struthers S. Environmental issues from coal mining and their solutions. Mining Science and Technology (China). 2010;20:215-223.

5.Finkelman RB. Potential health impacts of burning coal beds and waste banks. Int J Coal Geol. 2004;59:19-24.

6.Ribeiro J, Da Silva EF, Flores D. Burning of coal waste piles from Douro Coalfield (Portugal): petrological, geochemical and mineralogical characterization. Int J Coal Geol. 2010;81:359-372.

7.Xing Y, Feng J, Rong X. Discussion on causes of combustion and explosion and of coal gangue at the No. 4 mine of Pingdingshan coal Mine and countermeasures. Chinese J Geol Hazard Control. 2007;18:145-150.

8.Sloss LL. Assessing and managing spontaneous combustion of coal. Retrieved from London 2015

9.Querol X, Zhuang X, Font O, et al. Influence of soil cover on reducing the environmental impact of spontaneous coal combustion in coal waste gobs: a review and new experimental data. Int J Coal Geol. 2011;85:2-22.

10.Roy P, Guha A, Kumar KV. An approach of surface coal fire detection from ASTER and Landsat-8 thermal data: Jharia coal field, India. Int J Appl Earth Obs. 2015;39:120-127.

11.Pandey J, Kumar D, Mishra RK, et al. Application of thermography technique for assessment and monitoring of coal mine fire: a special reference to Jharia Coal Field, Jharkhand, India. Int. J. Adv. Remote Sensing GIS. 2013;2:138-147.

12.Chatterjee RS. Coal fire mapping from satellite thermal IR data – A case example in Jharia Coalfield, Jharkhand, India. Isprs J Photogramm. 2006;60:113-128.

13.Cracknell AP, Mansor SB. Detection of sub-surface coal fires using Landsat Thematic Mapper data. International Archives of Photogrammetry and Remote Sensing. 1993;29:750.

14.Misz-Kennan M, Tabor A. The thermal history of selected coal waste dumps in the Upper Silesian Coal Basin (Poland). Coal and Peat Fires: A Global Perspective. 2011;3

15.Carpentier O, Defer D, Antczak E, Duthoit B. The use of infrared thermographic and GPS topographic surveys to monitor spontaneous combustion of coal tips. Appl Therm Eng. 2005;25:2677-2686.

16.Xu Q, Huang B. Growth and physiological responses of creeping bentgrass to changes in air and soil temperatures. Crop Sci. 2000;40:1363-1368.
17.Kuroyanagi T, Paulsen GM. Mediation of high−temperature injury by roots and shoots during reproductive growth of wheat. Plant, Cell & Environment. 1988;11:517-523.
18.Zhang F, Zhou G. Estimation of canopy water content by means of hyperspectral indices based on drought stress gradient experiments of maize in the north plain China. Remote Sens-Basel. 2015;7:15203-15223.
19.El Bastawesy M, Ali RR, Deocampo DM, Al Baroudi MS. Detection and assessment of the waterlogging in the dryland drainage basins using remote sensing and GIS techniques. Ieee J-Stars. 2012;5:1564-1571.
20.Song Y, Wu C. Examining human heat stress with remote sensing technology. Gisci Remote Sens. 2018;55:19-37.
21.Mittler R. Abiotic stress, the field environment and stress combination. Trends Plant Sci. 2006;11:15-19.
22.Zhou X, Sun J, Tian Y, et al. Development of deep learning method for lead content prediction of lettuce leaf using hyperspectral images. Int J Remote Sens. 2020;41:2263-2276.
23.Caballero D, Calvini R, Amigo JM. Hyperspectral imaging in crop fields: Precision agriculture. In, Data handling in science and technology: Elsevier; 2020:453-473.
24.Cao Z, Wang Q, Zheng C. Best hyperspectral indices for tracing leaf water status as determined from leaf dehydration experiments. Ecol Indic. 2015;54:96-107.
25.Fang H, Liang S, Kuusk A. Retrieving leaf area index using a genetic algorithm with a canopy radiative transfer model. Remote Sens Environ. 2003;85:257-270.
26.Stagakis S, Markos N, Sykioti O, Kyparissis A. Monitoring canopy biophysical and biochemical parameters in ecosystem scale using satellite hyperspectral imagery: An application on a Phlomis fruticosa Mediterranean ecosystem using multiangular CHRIS/PROBA observations. Remote Sens Environ. 2010;114:977-994.
27.Sperdouli I, Moustakas M. Spatio‐temporal heterogeneity in Arabidopsis thaliana leaves under drought stress. Plant Biology. 2012;14:118-128.
28.Bowyer P, Danson FM. Sensitivity of spectral reflectance to variation in live fuel moisture content at leaf and canopy level. Remote Sens Environ. 2004;92:297-308.
29.Liu C, SUN P, Liu S. A review of plant spectral reflectance response to water physiological changes. Chinese Journal of Plant Ecology. 2016;40:80.
30.Yebra M, Dennison PE, Chuvieco E, et al. A global review of remote sensing of live fuel moisture content for fire danger assessment: Moving towards operational products. Remote Sens Environ. 2013;136:455-468.
31.Peñuelas J, Filella I, Biel C, Serrano L, Save R. The reflectance at the 950‐970 nm region as an indicator of plant water status. Int J Remote Sens. 1993;14:1887-1905.
32.Clevers JGPW, Kooistra L, Schaepman ME. Estimating canopy water content using hyperspectral remote sensing data. International Journal of Applied Earth Observation & Geoinformation. 2010;12:119-125.
33.de Jong SM, Addink EA, Doelman JC. Detecting leaf-water content in Mediterranean trees using high-resolution spectrometry. Int J Appl Earth Obs. 2014;27:128-136.
34.Yi Q, Wang F, Bao A, Jiapaer G. Leaf and canopy water content estimation in cotton using hyperspectral indices and radiative transfer models. Int J Appl Earth Obs. 2014;33:67-75.

35.Rodríguez-Pérez JR, Ordó Ez C, González-Fernández AB, et al. Leaf water content estimation by functional linear regression of field spectroscopy data. Biosyst Eng. 2018:S1375313746.
36.Ge Y, Bai G, Stoerger V, Schnable JC. Temporal dynamics of maize plant growth, water use, and leaf water content using automated high throughput RGB and hyperspectral imaging. Comput Electron Agr. 2016;127:625-632.
37.Rodríguez-Pérez JR, Ordóñez C, González-Fernández AB, et al. Leaf water content estimation by functional linear regression of field spectroscopy data. Biosyst Eng. 2018;165:36-46.
38.Virnodkar SS, Pachghare VK, Patil VC, Jha SK. Remote sensing and machine learning for crop water stress determination in various crops: a critical review. Precis Agric. 2020;21:1121-1155.
39.Yebra M, Quan X, Riaño D, et al. A fuel moisture content and flammability monitoring methodology for continental Australia based on optical remote sensing. Remote Sens Environ. 2018;212:260-272.
40.Yi Q, Bao A, Wang Q, Zhao J. Estimation of leaf water content in cotton by means of hyperspectral indices. Comput Electron Agr. 2013;90:144-151.
41.Krishna G, Sahoo RN, Singh P, et al. Comparison of various modelling approaches for water deficit stress monitoring in rice crop through hyperspectral remote sensing. Agr Water Manage. 2019;213:231-244.
42.Xiong X, Liu N, Wei Y, et al. Effects of non-uniform root zone salinity on growth, ion regulation, and antioxidant defense system in two alfalfa cultivars. Plant Physiol Bioch. 2018;132:434-444.
43.Wang J, Li X, Bai Z, Huang L. The effects of coal gangue and fly ash on the hydraulic properties and water content distribution in reconstructed soil profiles of coal‐mined land with a high groundwater table. Hydrol Process. 2017;31:687-697.
44.Tsai F, Philpot W. Derivative analysis of hyperspectral data. Remote Sens Environ. 1998;66:41-51.
45.Atzberger C, Darvishzadeh R, Immitzer M, et al. Comparative analysis of different retrieval methods for mapping grassland leaf area index using airborne imaging spectroscopy. International Journal of Applied Earth Observation & Geoinformation. 2015;43:S1544033316.
46.Peñuelas J, Pinol J, Ogaya R, Filella I. Estimation of plant water concentration by the reflectance water index WI (R900/R970). Int J Remote Sens. 1997;18:2869-2875.
47.Seelig HD, Hoehn A, Stodieck LS, et al. Plant water parameters and the remote sensing R 1300 / R 1450 leaf water index: controlled condition dynamics during the development of water deficit stress. Irrigation Sci. 2009;27:357-365.
48.Gao B. NDWI—A normalized difference water index for remote sensing of vegetation liquid water from space. Remote Sens Environ. 1996;58:257-266.
49.Rouse JW, Haas RH, Schell JA, Deering DW. Monitoring vegetation systems in the Great Plains with ERTS. NASA special publication. 1974;351:309.
50.DeFries RS, Townshend J. NDVI-derived land cover classifications at a global scale. Int J Remote Sens. 1994;15:3567-3586.
51.Jordan CF. Derivation of Leaf-Area Index from Quality of Light on the Forest Floor. Ecological Society of America. 1969
52.Wolf AF. Using WorldView-2 Vis-NIR multispectral imagery to support land mapping and feature extraction using normalized difference index ratios. In, Algorithms and Technologies for Multispectral, Hyperspectral, and Ultraspectral Imagery XVIII: International Society for Optics and Photonics; 2012:83900N.
53.Gamon JA, Peñuelas J, Field CB. A narrow-waveband spectral index that tracks diurnal changes in

photosynthetic efficiency. Remote Sens Environ. 1992;41:35-44.
54.Tibshirani R. Regression shrinkage and selection via the lasso. Journal of the Royal Statistical Society: Series B (Methodological). 1996;58:267-288.
55.Hochreiter S, Schmidhuber J. Long short-term memory. Neural Comput. 1997;9:1735-1780.
56.Kim J. Estimating classification error rate: Repeated cross-validation, repeated hold-out and bootstrap. Comput Stat Data an. 2009;53:3735-3745.
57.Anderson SA, Anderson WR. Ignition and fire spread thresholds in gorse (Ulex europaeus). Int J Wildland Fire. 2010;19:589-598.
58.Zhang W, Li X, Zhao L. A fast hyperspectral feature selection method based on band correlation analysis. Ieee Geosci Remote S. 2018;15:1750-1754.
59.Kramer PJ. Water stress research: progress and problems [Plant physiology]. 1983
60.Smart CM, Scofield SR, Bevan MW, Dyer TA. Delayed leaf senescence in tobacco plants transformed with tmr, a gene for cytokinin production in Agrobacterium. The Plant Cell. 1991;3:647-656.
61.Udomprasert N, Li PH, Davis DW, Markhart III AH. Effects of root temperatures on leaf gas exchange and growth at high air temperature in Phaseolus acutifolius and Phaseolus vulgaris. Crop Sci. 1995;35:490-495.
62.Zhang L, Zhou Z, Zhang G, et al. Monitoring the leaf water content and specific leaf weight of cotton (Gossypium hirsutum L.) in saline soil using leaf spectral reflectance. Eur J Agron. 2012;41:103-117.
63.Wu J, Chen TS, Pan LX. Spectrum Variance Analysis of Tree Leaves under the Condition of Different Leaf water Content. Guang pu xue yu Guang pu fen xi= Guang pu. 2015;35:1961-1966.
64.Cheng T, Rivard B, Sanchez-Azofeifa A. Spectroscopic determination of leaf water content using continuous wavelet analysis. Remote Sens Environ. 2011;115:659-670.
65.Dormann CF, Elith J, Bacher S, et al. Collinearity: a review of methods to deal with it and a simulation study evaluating their performance. Ecography. 2013;36:27-46.
66.Crisóstomo De Castro Filho H, Abílio De Carvalho Júnior O, Ferreira De Carvalho OL, et al. Rice crop detection using LSTM, Bi-LSTM, and machine learning models from Sentinel-1 time series. Remote Sens-Basel. 2020;12:2655.
67.Karim F, Majumdar S, Darabi H, Chen S. LSTM fully convolutional networks for time series classification. Ieee Access. 2017;6:1662-1669.

Figures

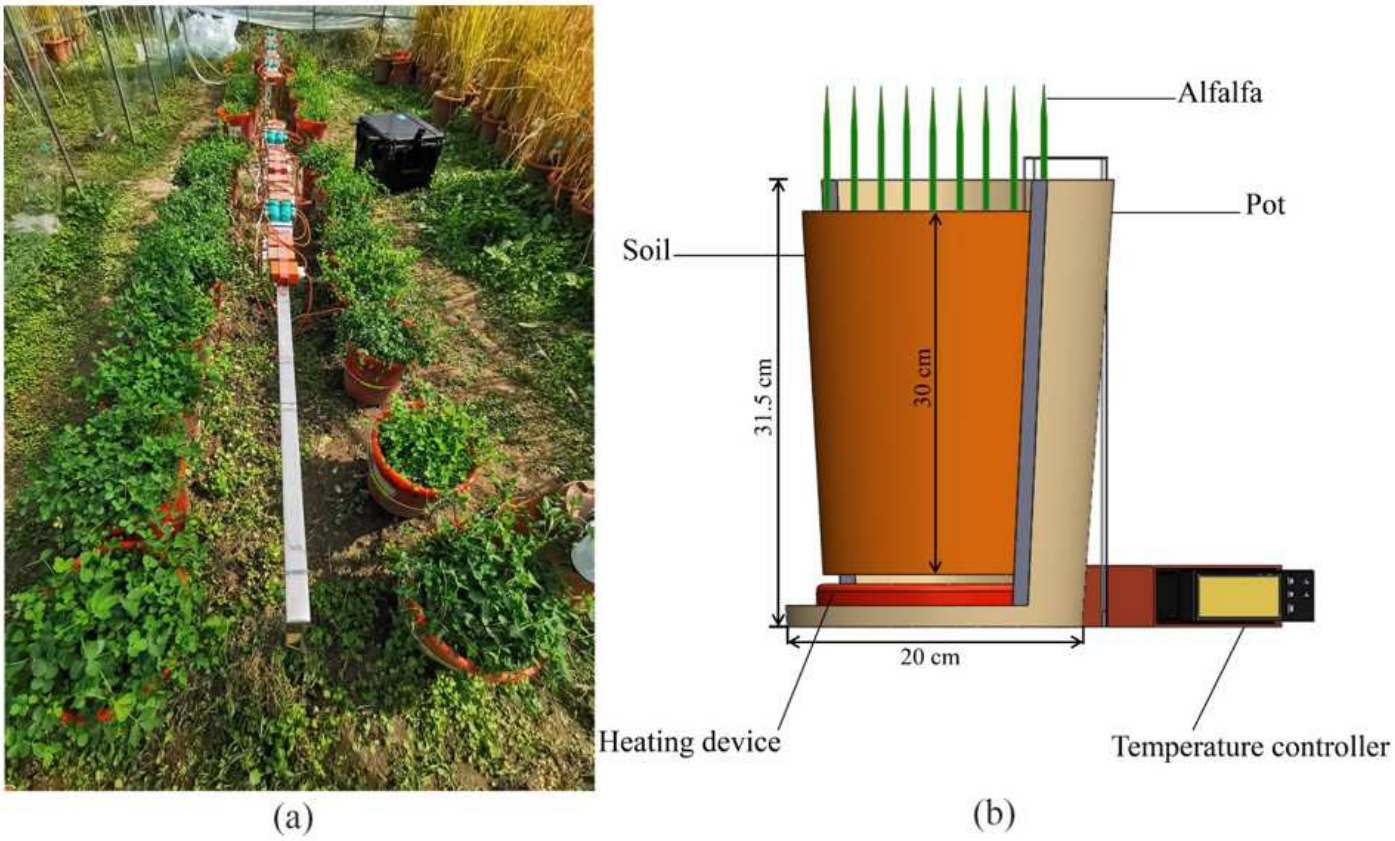

Figure 1

(a) Field of simulation experiment of heat stress in alfalfa and (b) schematic diagram of the heating equipment.

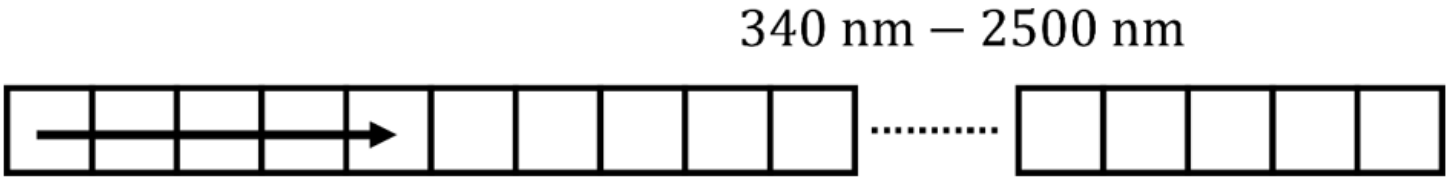

Figure 2

Schematic diagram of one-dimensional Gaussian filtering along the spectrum direction, with a sliding window of 5.

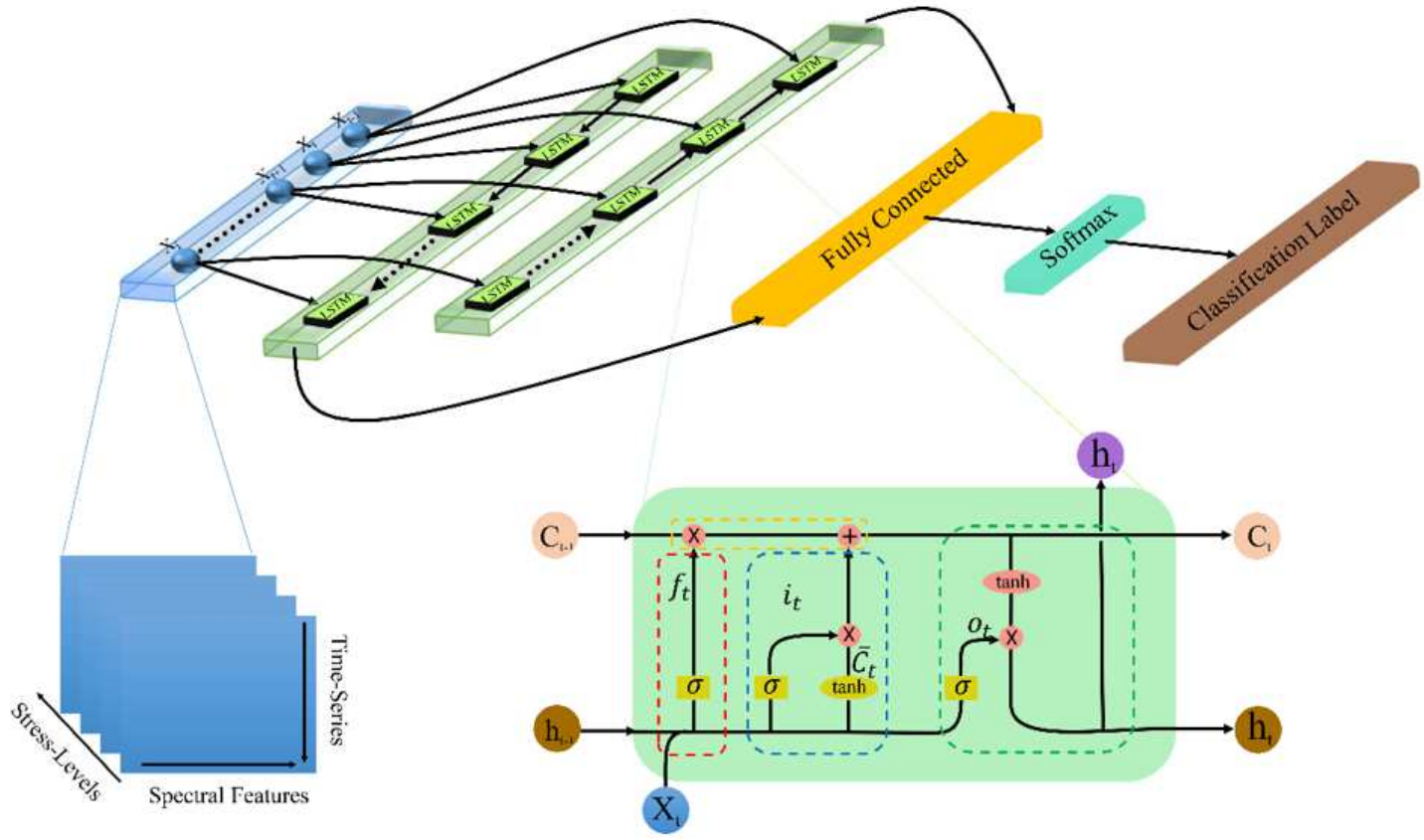

Figure 3

SF-LSTM network structure diagram.

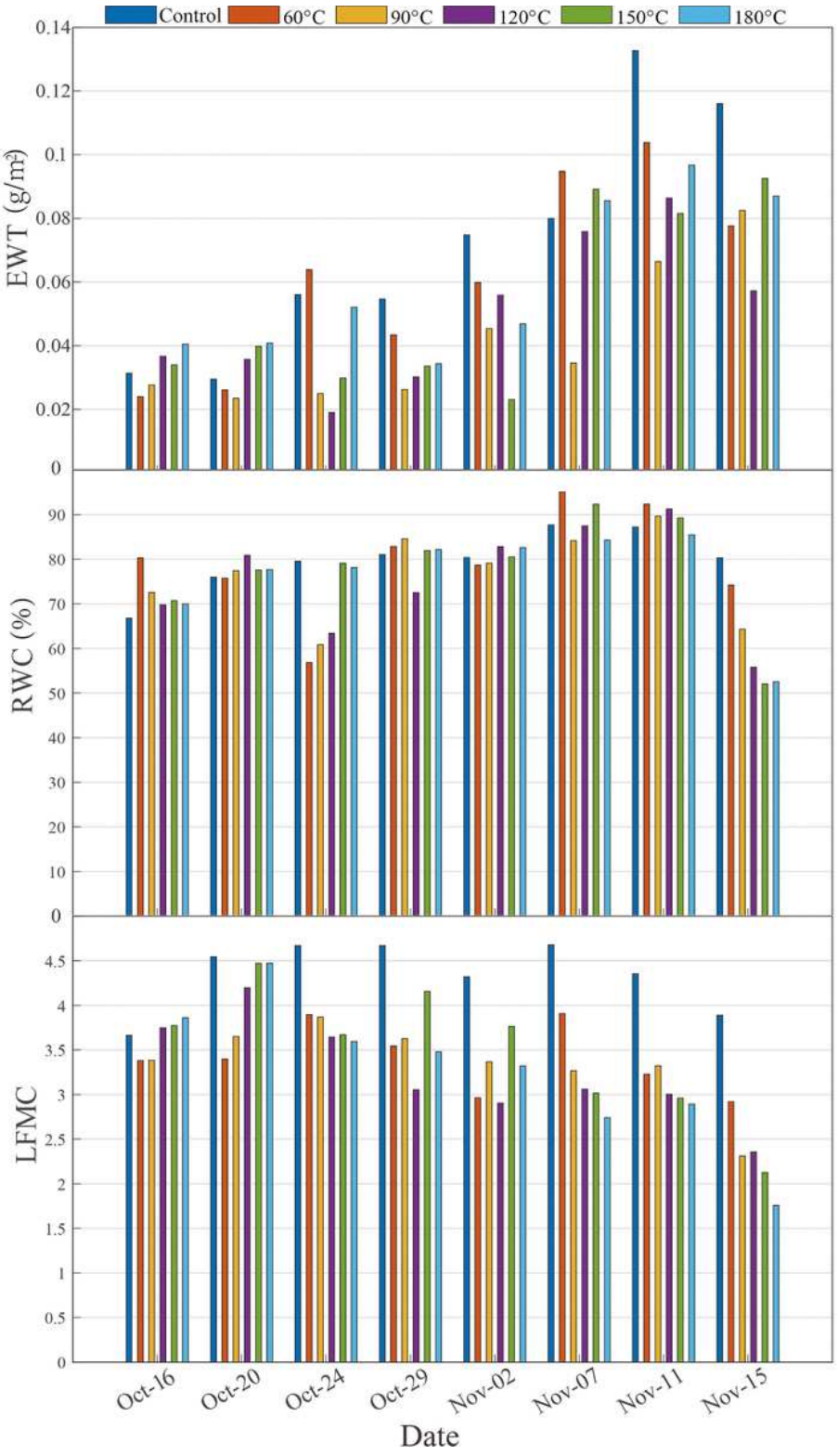

Figure 4

Time series of equivalent water thickness (EWT), live fuel moisture content (LFMC), and relative water content (RWC) in the control and experimental groups at leaf level from October 16–November 15, 2020.

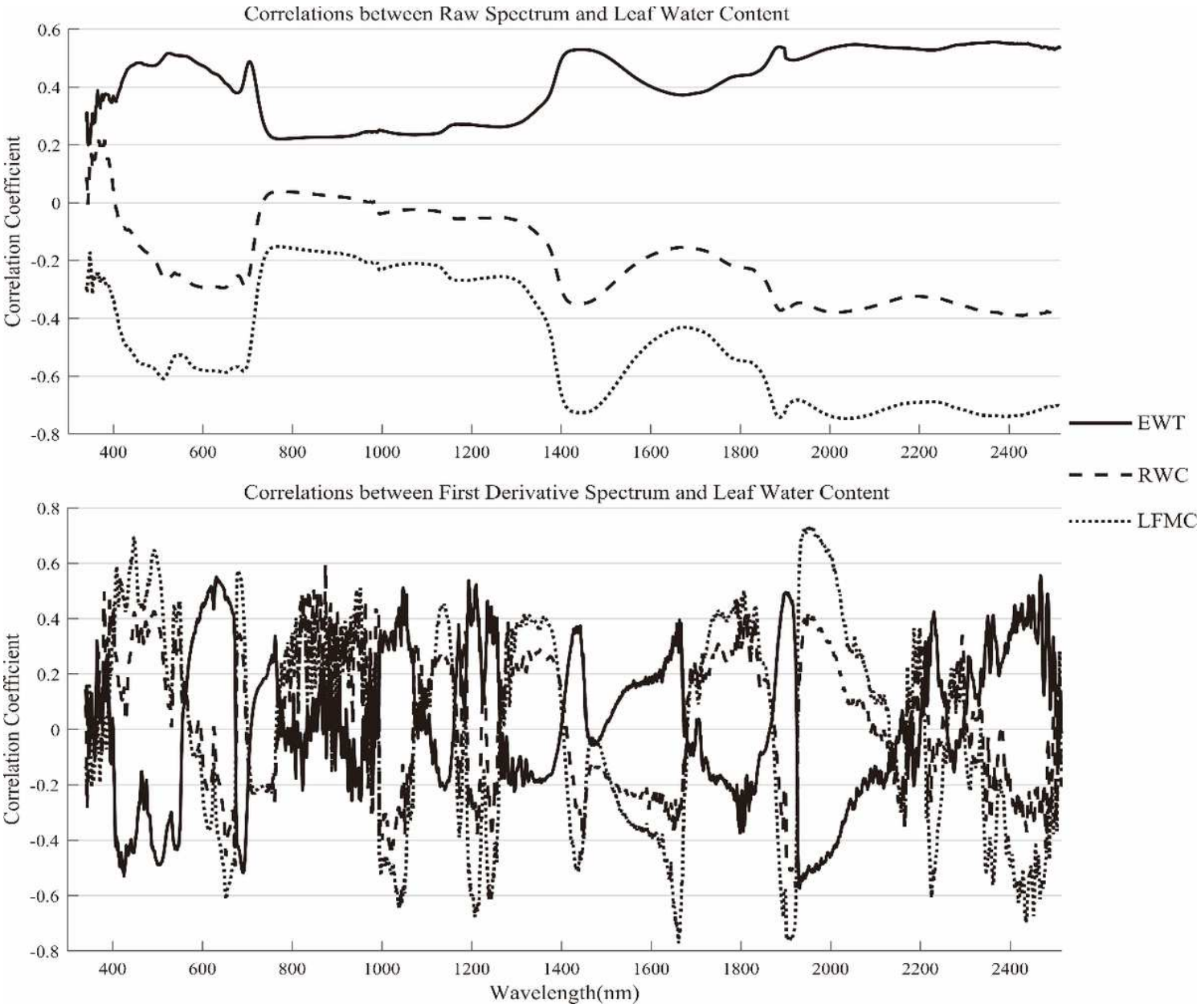

Figure 5

Coefficients of correlation between EWT, RWC, LFMC and the raw leaf and first-derivative spectral data

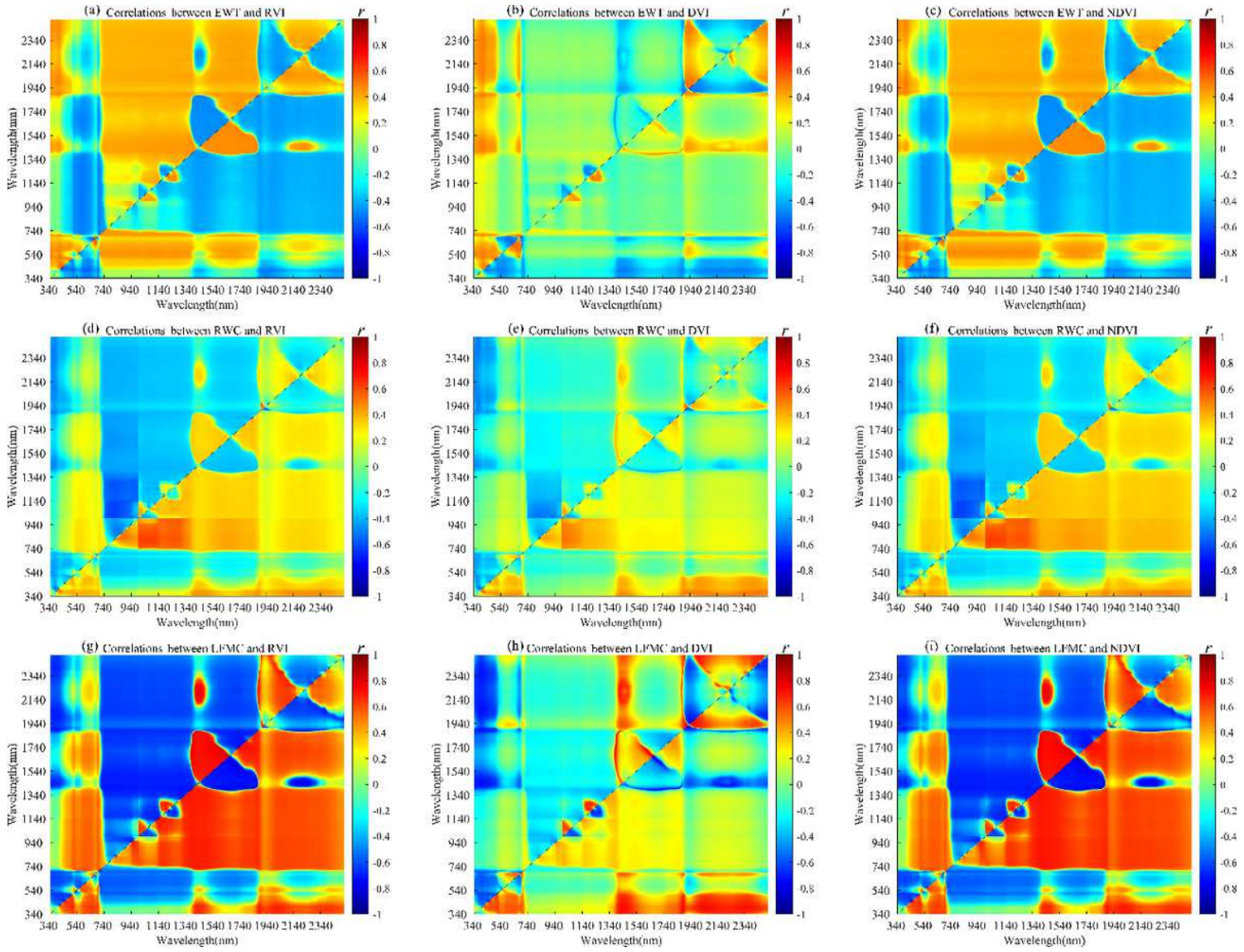

Figure 6

Coefficients of correlation between EWT, RWC, and LFMC with RVI (λ1, λ2), NDVI (λ1, λ2), DVI (λ1, λ2), and ratio/normalized difference/difference vegetation indexes constructed from raw spectral data

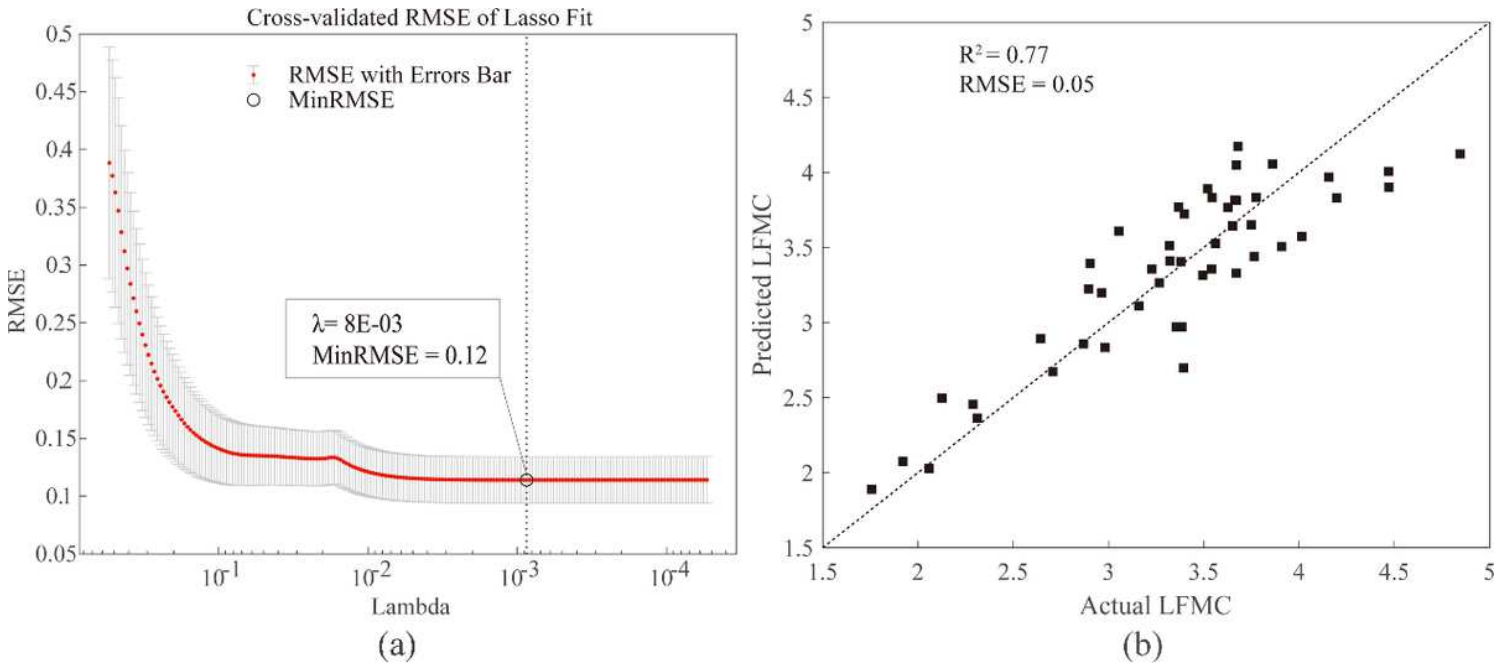

Figure 7

(a) Use of 10-fold cross-validation to determine the regular coefficient (lambda, λ) of the Lasso model; (b) predicted and actual values of LFMC by Lasso regression.

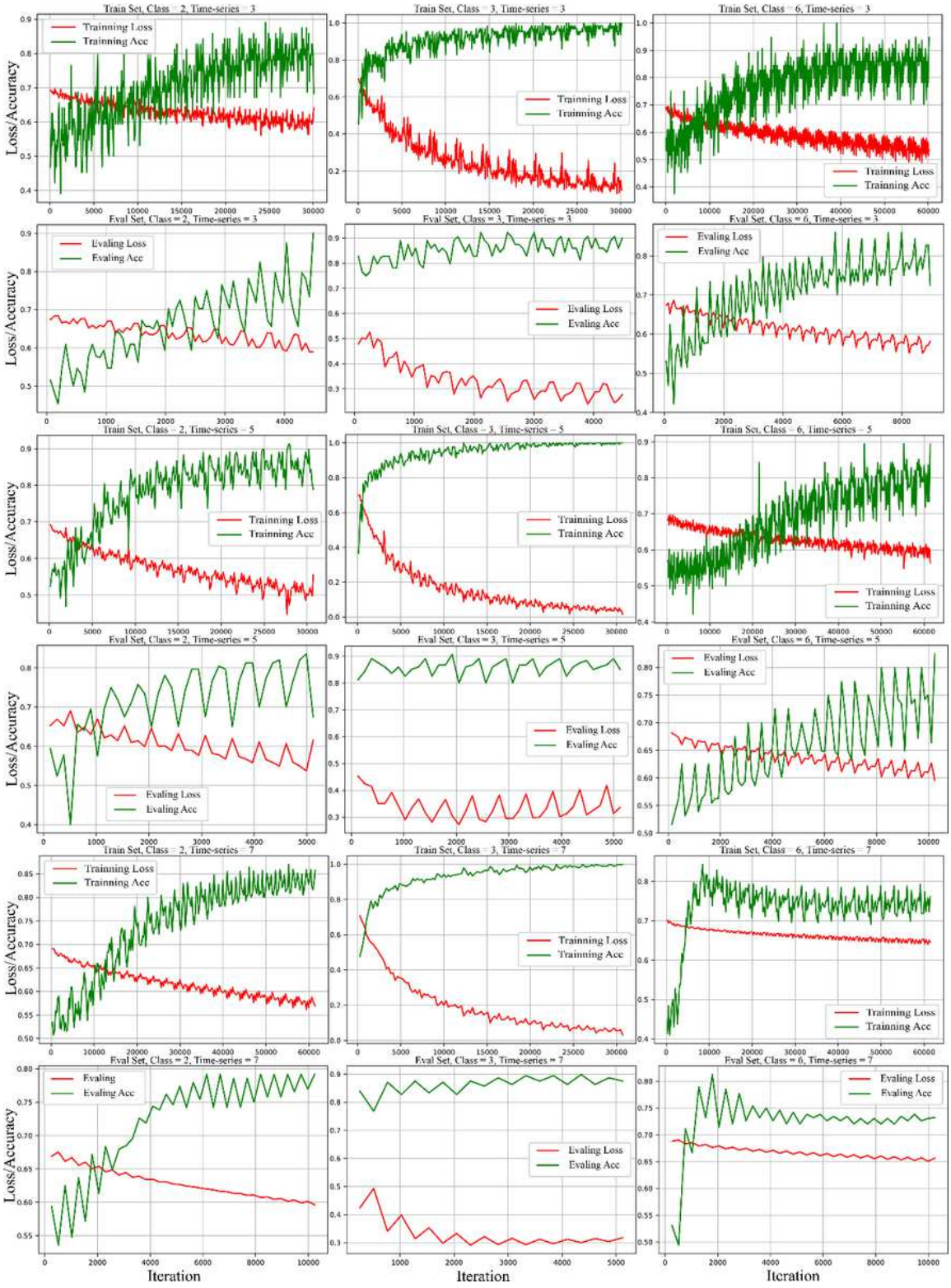

Figure 8

Loss and accuracy of the SF-LSTM model training set and validation set under different classification strategies and time series lengths